First-principles investigation of ReO_3 and related oxides

M. G. Stachiotti
Instituto de Física Rosario, Universidad Nacional de Rosario, 27 de Febrero 210 Bis, Rosario (2000), Argentina

F. Corà and C. R. A. Catlow
The Royal Institution of Great Britain, 21 Albemarle Street, London W1X 4BS, United Kingdom

C. O. Rodriguez
IFLYSIB, Grupo de Física del Sólido, Casilla de Correo 565, La Plata (1900), Argentina
(Received 18 July 1996; revised manuscript received 4 October 1996)

Electronic-structure calculations are performed, within the local-density approximation to the density-functional theory, using the full-potential linear muffin-tin orbital method to understand the relation between structural and electronic properties of ReO_3, WO_3, and the stoichiometric tungsten bronze $NaWO_3$. Energy changes associated with small deformations from the cubic phase indicate that ReO_3 and the tungsten bronze are stable when cubic while the W ion in WO_3 shows a tendency to off-center displacements. The different behavior is explained by examining the band structure of the compounds. Calculated frequencies and eigenvectors of Γ phonons in ReO_3 corroborate the existence of high-frequency modes in this crystal which supports a recent theoretical proposal for the interpretation of its electrical resistivity. [S0163-1829(97)03607-2]

I. INTRODUCTION

ReO_3 is a transition-metal oxide exhibiting high electrical conductivity. The Bravais lattice is simple cubic ($Pm3m$-O_h^1), with one formula unit ReO_3 per unit cell. Its structure comprises a network of corner-sharing oxygen octahedra, with Re occupying the center of each octahedron (Fig. 1). Among the numerous structures based on MO_6 corner sharing (including the perovskitelike compounds) ReO_3 is unusual in that the undistorted cubic structure is stable at all temperatures; however, a pressure-induced phase transition was discovered by Razavi, Altounian, and Datars,[1] who observed an anomaly in the Fermi surface when the sample was under pressure. Since then, the nature of this phase transformation has been investigated by different high-pressure experiments.[2–4]

In contrast to ReO_3, the closely related WO_3 shows several phase transitions and remains tetragonal up to the melting point: the distorted ReO_3 structure of WO_3 changes from tetragonal to orthorhombic, monoclinic, triclinic, and monoclinic during cooling.[5] On the other hand, when metal atoms are introduced in the WO_3 structure to form insertion compounds (the tungsten bronzes M_xWO_3), the cubic lattice is again stable for large values of x. In the stoichiometric tungsten bronze $NaWO_3$, the Na atom donates its $3s$ electron to the conduction band making $NaWO_3$ isoelectronic to ReO_3. Based on this simple anology, the stability of the cubic phase in ReO_3 could be associated with the occupancy of the conduction band, a point examined in this article. Fujimori and Tsuda have also attributed the different structural behavior to the screening effect involving W or Re $5d$ and O $2p$ states on the lattice vibrations.[6]

The band structure and Fermi surface of cubic ReO_3 were calculated semiempirically by Mattheiss[7] using the Slater-Koster linear combination of atomic orbitals scheme. The tight-binding parameters were adjusted to fit the optical and Fermi surface data. This work found that the valence and conduction bands are mainly composed of O $2p$ and Re $5d(t_{2g})$ orbitals, respectively. Strong bonding, due to the overlap of those states, contributes to the broadening of the $5d$ conduction band and leads to metallic conductivity. The Fermi surface is composed of two roughly spherical sheets centered about Γ plus a third sheet that consists of $\langle 100 \rangle$ directed cylinders intersecting at Γ. This remains, to our knowledge, the only theoretical investigation of the electronic structure of ReO_3.

There is a great deal of experimental information about dynamical properties of ReO_3, but a precise knowledge of the optical modes frequencies at the Brillouin zone center is still missing. The optical bond-stretching modes (Re-O) are observed in the region from 920 to 600 cm^{-1} and those assigned to the angle-bending modes (O-Re-O) are observed below 450 cm^{-1}. These modes have been probed by different techniques such as acoustic[8,9] electric conductivity,[10,11] and specific-heat[12,10] measurements; inelastic neutron[2] and Brillouin scattering;[13] and x-ray-absorption spectroscopy.[14] The

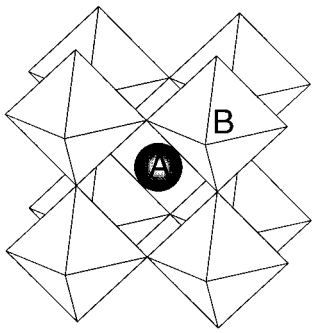

FIG. 1. Schematic representation of the perovskite structure ABO_3, showing the corner-sharing connection between oxygen octahedra. The dodecahedral site A is empty in the binary ReO_3 and WO_3 oxides, while it is occupied by Na in the bronze.

TABLE I. Basis set and MT-sphere radii used in the calculation.

Atom	$\kappa^2=-0.01$ Ry	$\kappa^2=-1.0$ Ry	$\kappa^2=-2.3$ Ry	R_{MT} (a.u.)
Re	$6s5p5d5f$	$6s5p5d$	$6s5p$	1.85
W	$6s5p5d4f$	$6s5p5d$	$6s5p$	1.85
O	$2s2p3d$	$2s2p$	$2s2p$	1.47
Na	$3s2p$	$3s$		3.2

only direct observation of optical phonons at the center of the Brillouin zone was made by IR transmission spectroscopy of ReO_3 films deposited upon a silicon plate.[15] Two peaks were found at room temperature at 905 and 315 cm^{-1} and assigned to the IR active stretching and bending modes, respectively, in agreement with the second-order Raman spectrum. Raman spectroscopy studies of tungsten oxides, with the ReO_3-like structure, confirm that the stretching and bending modes are expected at 800 and 270 cm^{-1}, respectively.[16,17]

In the present article, we report density-functional calculations of ReO_3, WO_3, and the stoichiometric tungsten bronze $NaWO_3$, performed with the full-potential linear muffin-tin orbital method. In Sec. II we give a description of the computational aspects of our study. The results are presented in Sec. III: the structure optimization and electronic structure in Sec. III A, the relation between the electronic structure and lattice stability in Sec. III B, and the calculation of frequencies and eigenvectors for the optical phonon modes at Γ in Sec. III C. Finally, Sec. IV contains a summary and conclusions.

II. METHOD OF CALCULATION

For the calculation of the electronic structure of the three oxides we used the full-potential (FP) linear muffin-tin orbital (LMTO) code by Methfessel,[18,19] within the local-density approximation (LDA) and the Hedin-Lundqvist exchange-correlation potential. In the FP-LMTO, no shape approximations are made for either the charge density or the potential. The participating states are divided into valence, semicore, and core. Core states are those confined within spheres centered on the nuclei. They are treated by solving the radial Schrödinger equation in each iteration, assuming that the wave function is zero on the sphere surface (unfrozen core). Semicore states are those associated with very narrow bands that can, however, spill out of the atomic sphere.

As is customary for a LMTO approach, the basis for the wave function consists of atom-centered Hankel functions, which are augmented by numerical solutions of the radial Schrödinger equation within the nonoverlapping atomic spheres. In the interstitial region the charge density is represented by fitting a linear combination of Hankel functions to the values and slopes on the sphere boundaries. To provide sufficient variational freedom, it is essential in the method to extend the basis using LMTO's with different localizations. The envelope function decays as $e^{-\kappa r}$, where $-\kappa^2$ is the kinetic energy of the Hankel function.

The FP-LMTO calculations were performed employing a basis set (presented in Table I) that was found to be optimal for describing the band structure of ReO_3. A similar setup was used in the study of the closely related ferroelectric perovskite $KTaO_3$.[20] In addition, Re $5s$ and W $5s$ states have been explicitly included in the separate semicore panel. The choice of muffin-tin (MT) radii was based on the spatial distribution of the self-consistent charge density over the unit cell; this allowed us to attribute charge densities centered at different atoms to their corresponding spheres, leaving only relatively smooth variations of the charge density over the interstitial region. The only exception is Na, whose sphere is enlarged in order to include some interstitial space around it. In the binary oxides, empty spheres (of radius $R_{MT}=3.2$ a.u.) were added at the dodecahedral sites in order to achieve better space filling. The resulting packing parameter (V_{MT}/V_{total}) was around 58%. The Brillouin-zone integrations were carried out by the tetrahedron method using 35 irreducible k points (corresponding to $8\times8\times8$ regular divisions along the k_x, k_y, and k_z axes, respectively).

TABLE II. Optimized cubic structures for ReO_3, WO_3, and $NaWO_3$. An asterisk denotes the Hartree-Fock (HF) calculation from Ref. 21.

Oxide	FP-LMTO (Å)	HF* (Å)	HF+correlation* (Å)	Expt. (Å)
ReO_3	3.71			3.75
WO_3	3.78	3.76	3.72	
$NaWO_3$	3.83			3.85

III. RESULTS

A. Structure optimization and electronic structure of ReO_3

Before analyzing the electronic properties, we have optimized the structure of the oxides examined. For the cubic phase this is a straightforward procedure: since the structure does not contain internal degrees of freedom, the change consists in an isotropic compression or expansion of the unit cell and corresponds to calculating the total energy as a function of the lattice parameter a. The results are shown in Table II. The equilibrium lattice constant for ReO_3, cubic WO_3, and $NaWO_3$ are 3.71, 3.78, and 3.83 Å, respectively. For ReO_3, the total energy as a function of volume has the minimum at $V/V_{expt}=0.969$. This difference in the evaluation of the equilibrium volume is typical for a calculation using the local-density approximation. As cubic WO_3 has never been observed experimentally, we compare our results with Hartree-Fock calculations.[21] There is good agreement for the equilibrium lattice constants obtained with the two techniques. For $NaWO_3$ we compare the equilibrium lattice constant with the estimate given by the empirical formula $a=3.7899$ Å$+0.0601$ Å$\times x$ [valid for Na_xWO_3 when $x>0.75$ (Ref. 22)] for $x=1$. Results of the calculations reported hereafter make reference to the optimized cubic structure of ReO_3. For subsequent reference, we define a_0 as the calculated equilibrium lattice constant of ReO_3 ($a_0=3.71$ Å).

The calculated band structure for ReO_3 is shown in Fig. 2(a) [Fig. 2(b) is for further reference]. Here and in the following figures the zero of energy is chosen to coincide with the Fermi level of the solid in the case of metallic behavior and the top of the valence band if it is an insulator. The general features are not greatly different from the earlier tight-binding (TB) calculation;[7] there are, however, appre-

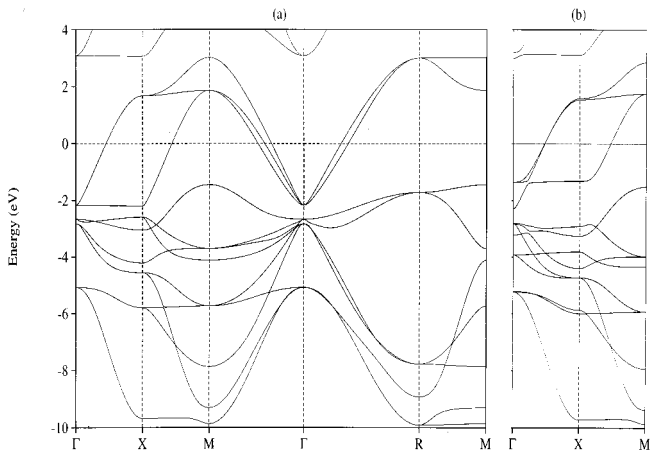

FIG. 2. (a) Band structure of ReO_3. (b) Band structure along the Γ-X-M direction for distorted ReO_3. In the distorted structure the Re ion is displaced by 3% of the lattice constant a_0 along the [001] direction.

ciable differences in bandwidths and band gaps. In our calculation, the widths of the conduction and valence bands are approximately 5 and 8 eV, respectively. These values are greater than the 4 and 6.5 eV obtained in Ref. 7. The oxygen $2s$ bands are centered at $\approx$20 eV below the Fermi level and have a bandwidth of 2.8 eV. In the TB band structure there is a gap between the conduction and valence bands unlike our calculations, where the top of the valence band at the M point overlaps the energy range of the conduction band. The conduction band presents splittings along the Γ-R and Γ-M directions, which are particularly important for the determination of the Fermi surface and that influence the conductivity of the solid. To obtain similar splittings in the TB calculation it was necessary to introduce a spin-orbit parameter that was determined by comparison between the theoretical and experimental Fermi-surface areas. This effect arises in our calculation without including spin-orbit coupling.

In Fig. 3 we report the band structure, projected onto the basis set associated with the atomic MT spheres, along the Γ-X-M directions. The shaded width is proportional to the partial change of the specified atom and orbital and allows us

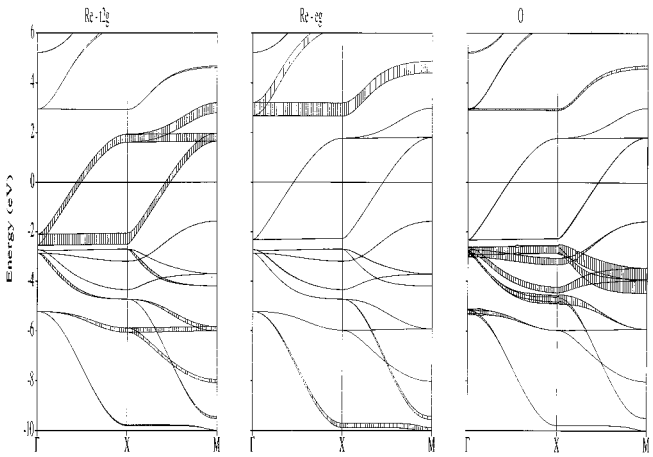

FIG. 3. Projected band structure of ReO_3 indicating the contributions to each band along the Γ-X-M directions.

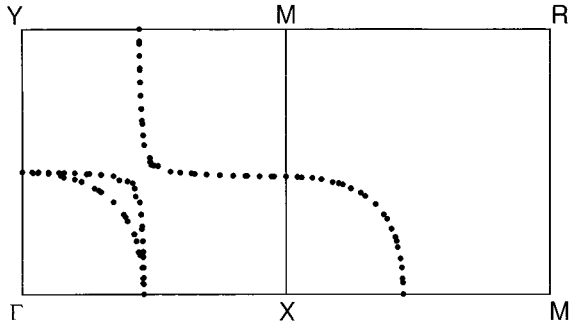

FIG. 4. Fermi surface of ReO_3 on the $k_z=0$ and $k_x=\pi/a$ planes of the Brillouin zone.

to highlight the contributions from the Re and oxygen orbitals of a particular symmetry to each band. The valence band is formed mainly by O $2p$ states, although they are strongly hybridized with Re $5d$ orbitals. The conduction band has a dominant contribution from the Re $5d(t_{2g})$ orbitals, while the Re $5d(e_g)$ orbitals lie at higher energy. This trend in the band composition closely resembles that obtained for cubic WO_3 in Ref. 21. The same arguments advanced there apply to the case of ReO_3 treated here: mixing of oxygen and metal states occurs in both valence and conduction bands, but we can clearly distinguish a dominant contribution from the oxygens in the valence band and from the metal in the conduction band (partly occupied in the case of the metallic ReO_3). Regarding the relative energy ordering of the metal e_g and t_{2g} levels, we note that in the conduction band this is as expected for a metal ion in a octahedral field, with the t_{2g} levels at lower energy. The metal contribution in the valence band takes into account the hybridization of its states with the surrounding oxygens. The stabilization arising from this interaction is proportional to the overlap of the corresponding orbitals; this is maximum for the e_g orbitals, which point directly towards the oxygen p states, and the resulting stabilization is such that the e_g levels lie at lower energy than the t_{2g} in the valence band.

Figure 4 shows the calculated Fermi surfaces on the $k_z=0$ and $k_x=\pi/a$ planes. Two out of the three sheets are closed surfaces centered about Γ, with completely electronlike character. The third is an open surface, with both electronlike and holelike character, and consists of $\langle 100\rangle$ directed cylinders intersecting at Γ. The shape of the three surfaces agrees with the ones obtained by Mattheiss[7] by adjusting the tight-binding parameters to fit the de Haas–van Alphen data of Marcus.[23]

B. Relation between electronic structure and lattice stability of ReO_3, WO_3, and $NaWO_3$

The electronic band structures for the optimized unit cells of cubic WO_3 and $NaWO_3$ are shown in Figs. 5(a) and 5(b), respectively; they are very similar to the results of earlier calculations performed on $NaWO_3$ within the atomic sphere approximation (LMTO) atomic sphere approximation.[24] We note that the band structures of the three oxides are topologically very similar (compare with Fig. 2 for ReO_3). Because of the different number of valence electrons per unit cell, the conduction band is empty in WO_3 and half filled in ReO_3 and

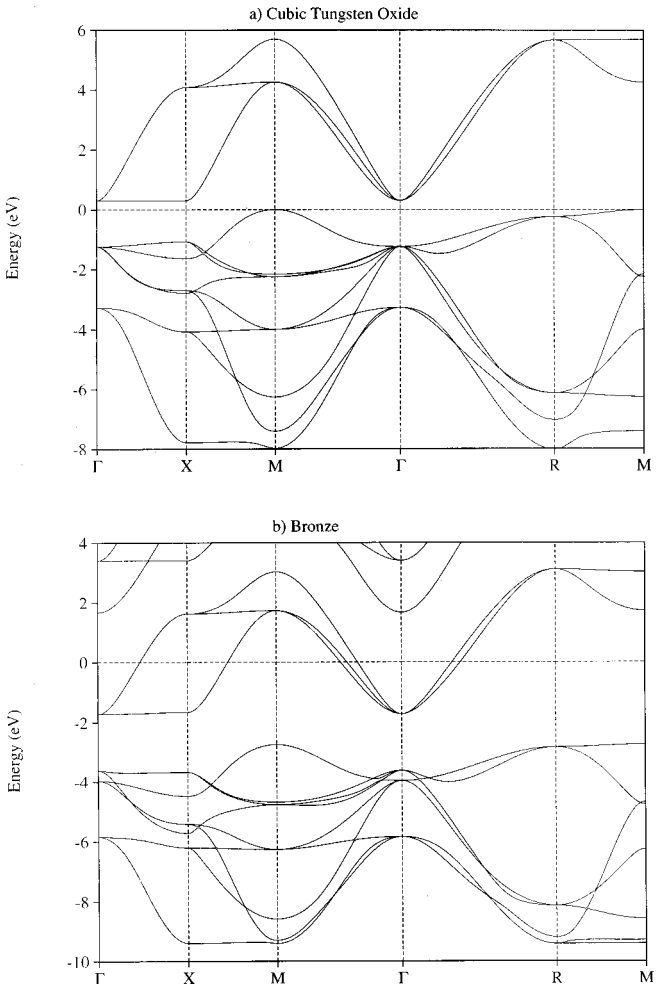

FIG. 5. Band structure of (a) cubic WO_3 and (b) stoichiometric tungsten bronze $NaWO_3$.

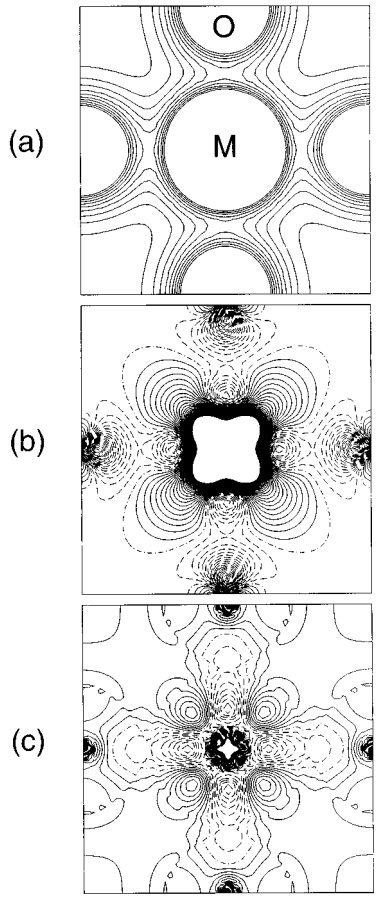

FIG. 6. (a) Valence charge density of ReO_3 and (b) and (c) difference between the self-consistent charge density for the metals and WO_3 in the (100) plane: (b) ReO_3 and (c) $NaWO_3$. Continuous, dashed, and dot-dashed lines correspond to positive, negative, and zero densities, respectively; the interval between consecutive isodensity lines is 0.0015 a.u. (e/bohr^3).

the tungsten bronze. The latter two materials are therefore metallic conductors, while the former is an insulator, in agreement with the experimental evidence.[25] This, together with the agreement already mentioned with the experimentally determined Fermi surface for the case of ReO_3, reassures that for our case the LDA gives reliable predictions for the band structures. As in ReO_3, in both WO_3 and $NaWO_3$ the valence bands have a prevalent contribution from the O $2p$ orbitals and the conduction bands from the metal t_{2g} orbitals.

The charge density in ReO_3 was investigated experimentally by x-ray structural analysis.[26] An anisotropic charge distribution was found around the Re atom, which was attributed to the π bond formed by Re $5d(t_{2g})$ and O $2p$ electrons. This experiment also indicated that the thermal vibrations of the oxygen atoms were remarkably anisotropic at every temperature: the amplitude of the oxygen vibration towards Re is in fact much smaller than in the perpendicular direction, towards the empty spaces of the perovskitelike structure. These structural features of the solid are evident in Fig. 6(a), where we show the calculated valence charge density of ReO_3 in the (001) plane. The metal and oxygen positions marked in Fig. 6(a) serve as a reference for Figs. 6(b) and 6(c).

The electronic charge densities for WO_3 and $NaWO_3$ are very similar to the one shown in Fig. 6(a) for ReO_3. To highlight the differences we have compared the valence density of both metals with that obtained for WO_3. Figure 6(b) reports the difference between ReO_3 and WO_3 in the (100) plane. In both cases we have employed the equilibrium lattice parameter of ReO_3 (a_0). Given the similarity in the band structures, this procedure can be considered as equivalent to integrating the density of the half-filled conduction band in ReO_3 (showing also a minor charge redistribution arising from the different potentials of the two crystals); this map is therefore showing the distribution of the electron responsible for the metallic conductivity of ReO_3. The corresponding difference density map for $NaWO_3$ is shown in Fig. 6(c). In ReO_3 the conduction electron is well localized in a t_{2g} orbital on the metal center; this is not the case in the bronze, where the electron is delocalized over the whole structure. In both cases we observed a depopulation of the metal e_g orbital. The plane selected in Fig. 6 does not contain Na ions; the increased density at the corners of Fig. 6(c), with respect to Fig. 6(b), therefore is not directly associated with the Na nuclear region. The Na cations in the bronze increase the polarization of the oxygen ions in the direction perpendicular to W-O, as can be seen in Fig. 6(c).

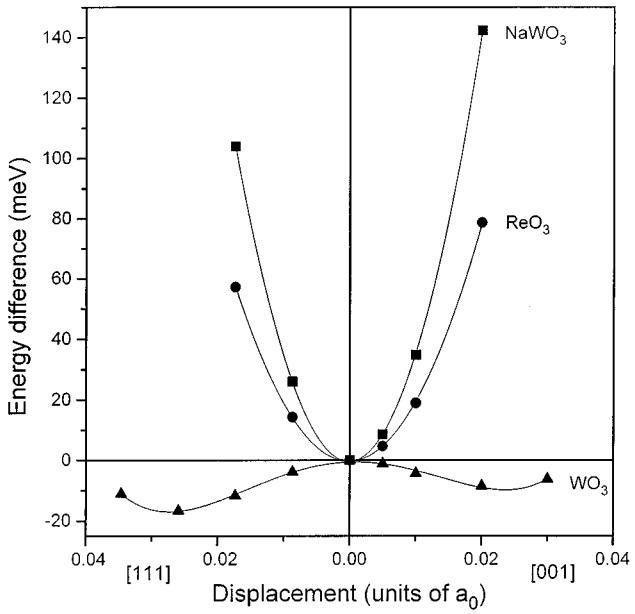

FIG. 7. Total energy versus transition-metal displacements along the [001] (right) and [111] (left) directions for ReO_3, $NaWO_3$, and WO_3.

In the study of the lattice deformations we are interested in understanding the different behaviors of the three materials and not their absolute properties. For this reason we did not consider completely optimized structures, but used an idealized description in which the oxygen sublattice is fixed in its undistorted cubic position. The lattice parameter chosen was a_0 in every case. Only ferroelectric displacements of the transition metal along the principal crystallographic directions have been examined: results are shown in Fig. 7, where the total energy is reported for displacements of the transition metal sublattice along the [001] (right panel) and [111] (left panel) directions. These movements correspond to displace the B ion towards a corner ([001]) or towards a face ([111]) of its coordination octahedron (see Fig. 1). For ReO_3 and the bronze, the cubic structure remains favored over the displaced ones and the potential wells have an essentially parabolic shape. On the contrary, the cubic structure in WO_3 is unstable when the transition metal is displaced, in both the [001] and [111] directions; the equilibrium position for W is along the [111] direction, and a local minimum exists also in the [001]. The energy gained from the displacements is 16.7 and 8.5 meV, respectively.

One important contribution explaining the different behavior arises from the one-electron part of the total energy. In Fig. 2(b) we report the band structure of distorted ReO_3, where the Re sublattice is displaced by 3% of the lattice constant a_0 along the [001] direction; the same qualitative effects occur for the other two materials. Under displacement of the transition metal, both valence and conduction bands are distorted; in particular, we observe a stabilization in the valence band and a destabilization of the conduction band. Two of the six valence bands ranging from -2.6 to -4.5 eV are stabilized at a lower energy; on the other hand, the flat conduction band in the Γ-X direction, that lies in the region of ≈ -2 eV is destabilized by ≈ 0.9 eV.

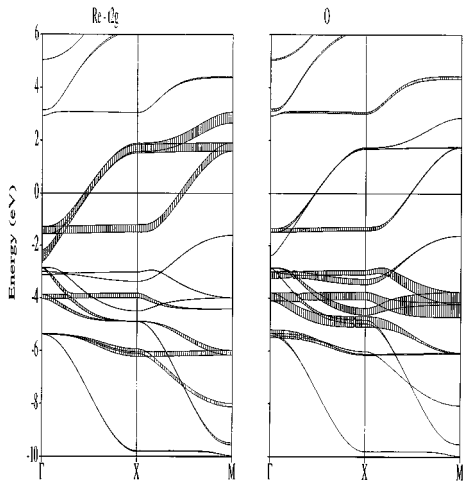

FIG. 8. Projected band structure for distorted ReO_3 indicating the contributions to each band along the Γ-X-M directions. In the distorted structure the Re ion is displaced by 3% of the lattice constant a_0 along the [001] direction.

To illustrate the origin of the above splitting in the energy levels, we make reference to Fig. 8. It corresponds to the projected band structure of Fig. 3, after the displacement of the Re ion. In the cubic phase, the two flat bands between -3 and -2 eV that represent the top of the valence band and the bottom of the conduction band along the Γ-X direction correspond to pure O $2p$ and Re $d(t_{2g})$ states (see Fig. 3). The transition-metal displacement causes a hybridization of the two levels, with bonding character in the valence band and antibonding in the conduction band. In Fig. 8, in fact, we clearly see that after the displacement of Re, the levels described above have contributions from both O $2p$ and Re $d(t_{2g})$. The atomic orbitals involved have π symmetry along the Re-O direction; we can therefore ascribe the changes to the onset of a π bond between metal and oxygen. In WO_3 only the bonding level is filled and the distortion is energetically stable, while in the metallic oxides ReO_3 and $NaWO_3$ also the antibonding orbital is populated; this second effect destabilizes the distorted structure of the latter materials and opposes the deformations examined.

A similar hybridization pattern between the transition metal and oxygen states was found to be essential to explain the ferroelectric behavior of ternary perovskites;[27,20] a more detailed study of the effects of charge distortion and covalence in WO_3 is reported in Ref. 21, where the importance of the W-O hybridization for the stability of the tetragonal phase is discussed in detail.

C. Frozen phonon calculation in ReO_3

As we have pointed out in Sec. III A, the value calculated from the total-energy minimum for the equilibrium volume of cubic ReO_3 is $\approx 0.97\%$ of the experimental cell volume. Such a discrepancy is known to be typical for calculations based on the LDA. Since the curvature of the total-energy hypersurface may be affected by the error in the cell volume and LDA calculations generally agree best with experiment when performed at the experimental lattice parameter, we

TABLE III. Frequencies and eigenvectors in ReO_3.

Symmetry	Eigenvectors Re	O_1	O_2	O_3	Frequency (cm^{-1})
			$a=3.71$ Å		
$F_{1\mu}$	−0.84	0.54	0.54	0.02	222
$F_{1\mu}$	0.16	0.29	0.29	−0.94	822
$F_{2\mu}$	0	1	−1	0	438
			$a=3.75$ Å		
$F_{1\mu}$	−0.85	0.52	0.52	0.05	217
$F_{1\mu}$	0.14	0.32	0.32	−0.94	760
$F_{2\mu}$	0	1	−1	0	433

performed our phonon calculation for both the theoretical ($a_0=3.71$ Å) and the experimental ($a=3.75$ Å) values of the lattice constant.

As is known (see, e.g., Ref. 15), Γ phonon vibration modes in the cubic perovskite structure of ReO_3 are split by symmetry into two $F_{1\mu}$ modes and one $F_{2\mu}$ mode (all of which are triply degenerate). The $F_{1\mu}$ modes are active only in the infrared, while the $F_{2\mu}$ mode is inactive in both the infrared and Raman spectra (silent mode).

In the cubic cell we have a Re atom at (0,0,0), an oxygen atom at (a/2,0,0) (O_1), a second oxygen atom at (0,a/2,0) (O_2), and a third oxygen atom at (0,0,a/2) (O_3). Since the modes at Γ are degenerate with respect to displacements in the x, y, or z direction, it is convenient to select a reference one say z, where atoms are displaced by an amount u. Symmetry requires that $u(O_1)=u(O_2)$ in the $F_{1\mu}$ modes and $u(O_1)=-u(O_2)$ in the $F_{2\mu}$ mode. To provide a good multidimensional fit of the total-energy hypersurface in the evaluation of phonon frequencies, we have performed total-energy calculations for 22 and 4 different displacement patterns (which include individual atoms as well as mixed displacements) for the infrared $F_{1\mu}$ and silent $F_{2\mu}$ modes, respectively. Atomic displacements were extended up to 3% of the lattice constant. A second-order least-squares fit was applied, and the phonon frequencies and eigenvectors were derived.

The frequencies and eigenvectors for both theoretical and experimental cubic structures are shown in Table III. Despite the differences in the calculated frequencies, the corresponding relative displacements of atoms determined for both lattice constants are very close. As can be seen from the eigenvectors, the high-frequency $F_{1\mu}$ mode is a Re-O stretching mode that involves a displacement of O_3 with respect to the rest of the crystal. The low-frequency $F_{1\mu}$ mode and the silent mode are O-Re-O bending modes. The difference in the calculated frequencies for these two bending modes can be understood examining their respective eigenvectors: while the silent is a pure oxygen mode, the bending $F_{1\mu}$ mode includes an important contribution from Re displacement. Due to the large mass of Re, the frequency of the bending $F_{1\mu}$ mode is smaller.

The calculated frequencies for the two infrared active modes are lower than the ones obtained by IR transmission spectroscopy of ReO_3 film,[15] where two peaks were found at room temperature at 905 and 315 cm^{-1}. It is not possible to ascertain whether such a discrepancy arises from errors due to the LDA or from the fact that the experimental results are obtained for the thin films and therefore are not a valid model for the bulk system. However, the present calculation corroborates a very important fact: the existence of a high-frequency stretching mode ($\omega\approx800$ cm^{-1}) in ReO_3.

The existence of high-energy phonons in ReO_3 is particularly interesting. Allen and Schulz[28] analyzed the shape and magnitude of the electrical resistivity for four inter-metallic compounds. They concluded that ReO_3 belongs to the normal class of conventional band Fermi liquids, with electron-phonon interactions dominating the resistivity, but showing a sharp departure from the Bloch-Grüneisen formula that could be explained if most of the phonons coupling involves high-frequency vibrations.

IV. SUMMARY

We have presented *ab initio* calculations of the band structure and Fermi surface of metallic ReO_3. Despite the differences in the calculated bandwidths and band gaps, the general features of the band structure and Fermi surface are not very different from those obtained in an earlier LCAO calculation, where the tight-binding parameters were adjusted to fit the optical and de Haas–van Alphen data.

The differences in structural behavior between WO_3 and the metallic compounds ReO_3 and $NaWO_3$ have been studied by performing total-energy calculations. The energy changes associated with small deformations from the cubic phase indicate that ReO_3 and the tungsten bronze are stable when cubic, while off-center displacements of the metal ion are stable in WO_3. The different behavior is explained by the strong destabilization of the conduction band that follows the displacement of the transition metal ion. In WO_3 the conduction band is vacant and a stabilization of the valence band due to the Wd–O p hybridization favors the distorted structure, while in ReO_3 and $NaWO_3$ the destabilizing effect due to the occupation of the conduction band prevails, opposing the deformations. Finally, a frozen phonon calculation of Γ phonons in ReO_3 corroborated the existence of a high-frequency Re-O stretching mode.

ACKNOWLEDGMENTS

M.G.S. gratefully acknowledges support (by a grant) from Consejo Nacional de Investigaciones Científicas y Técnicas de la República Argentina and Consejo de Investigaciones de la Universidad Nacional de Rosario. F.C. would like to acknowledge support from ICI Katalco and Molecular Simulations Inc.

[1] F. S. Razavi, Z. Altounian, and W. R. Datars, Solid State Commun. **28**, 217 (1978).
[2] J. D. Axe, Y. Fujii, B. Batlogg, M. Greenblatt, and S. Di Gregorio, Phys. Rev. B **31**, 663 (1985).
[3] J.-E. Jorgensen, J. D. Jorgensen, B. Batlogg, J. P. Remeika, and J. D. Axe, Phys. Rev. B **33**, 4793 (1986).
[4] B. Houser, R. Ingalls, and J. J. Rehr, Physica B **208-209**, 323 (1995).
[5] E. Salje, Acta Crystallogr. B **33**, 547 (1977).
[6] A. Fujimori and N. Tsuda, Solid State Commun. **34**, 433 (1980).
[7] L. F. Mattheiss, Phys. Rev. **181**, 987 (1969).
[8] T. P. Pearsall and L. A. Coldren, Solid State Commun. **18**, 1093 (1976).
[9] N. Tsuda, Y. Sumino, I. Ohno, and T. Akahane, J. Phys. Soc. Jpn. **41**, 1153 (1976).
[10] C. N. King, H. C. Kirsch, and T. H. Geballe, Solid State Commun. **9**, 907 (1971).
[11] T. Tanaka, T. Akahane, E. Bannai, S. Kawai, N. Tsuda, and Y. Ishizawa, J. Phys. C. **9**, 1235 (1976).
[12] F. C. Zumsteg and T. P. Pearsall, Solid State Commun. **16**, 751 (1975).
[13] R. E. Benner, E. M. Brody, and H. R. Shanks, J. Solid State Chem. **22**, 361 (1977).
[14] G. Dalba, P. Fornasini, A. Kuzmin, J. Purans, and F. Rocca, J. Phys. Condens. Matter **7**, 1199 (1995).
[15] M. Ishii, T. Tanaka, T. Akahane, and N. Tsuda, J. Phys. Soc. Jpn. **41**, 908 (1976).
[16] J. Wu and S. Li, J. Phys. Chem. **99**, 4566 (1995).
[17] M. F. Daniel, B. Desbat, J. C. Lassegues, B. Gerand, and M. Figlarz, J. Solid State Chem. **67**, 235 (1987).
[18] M. Methfessel, Phys. Rev. B **38**, 1537 (1988).
[19] M. Methfessel, C. O. Rodriguez, and O. K. Andersen, Phys. Rev. B **40**, 2009 (1989).
[20] A. V. Postnikov, T. Neumann, G. Borstel, and M. Methfessel, Phys. Rev. B **48**, 5910 (1993); A. V. Postnikov, T. Neumann, and G. Borstel, *ibid*. **50**, 758 (1994).
[21] F. Corà, A. Patel, N. Harrison, R. Dovesi, and C. R. A. Catlow, J. Am. Chem. Soc. (to be published).
[22] Powder Diffraction File, International Centre for Diffraction Data, Sets 27 and 28, 28-1156, p. 906.
[23] S. M. Marcus, Phys. Lett. **27A**, 584 (1968).
[24] N. E. Christensen and A. R. Mackintosh, Phys. Rev. B **35**, 8246 (1987).
[25] A. Ferreti, D. Rogers, and J. Goodenough, J. Phys. Chem. Solids **26**, 2007 (1965).
[26] M. Morinaga, K. Sato, J. Harada, H. Adachi, S. Ohba, and Y. Saito, J. Phys. C **16**, L177 (1983).
[27] R. Cohen, Nature **358**, 136 (1992).
[28] P. B. Allen and W. W. Schulz, Phys. Rev. B **47**, 14 434 (1993).